J|A|C|S ARTICLES

Published on Web 07/31/2009

^{31}P MAS Refocused INADEQUATE Spin−Echo (REINE) NMR Spectroscopy: Revealing *J* Coupling and Chemical Shift Two-Dimensional Correlations in Disordered Solids

Paul Guerry,† Mark E. Smith, and Steven P. Brown*

Department of Physics, University of Warwick, Coventry CV4 7AL, U.K.

Received March 21, 2009; E-mail: s.p.brown@warwick.ac.uk

Abstract: Two-dimensional (2D) variations in $^2J_{P_1,P_1}$, $^2J_{P_1,P_2}$, and $^2J_{P_2,P_2}$ are obtained—using the REINE (*RE*focused *IN*ADEQUATE spin−*E*cho) pulse sequence presented by Cadars et al. (*Phys. Chem. Chem. Phys.* **2007**, *9*, 92−103)—from pixel-by-pixel fittings of the spin−echo modulation for the 2D correlation peaks due to linked phosphate tetrahedra (P_1-P_1, P_1-P_2, P_2-P_1, and P_2-P_2) in a ^{31}P refocused INADEQUATE solid-state MAS NMR spectrum of a cadmium phosphate glass, $0.575CdO-0.425P_2O_5$. In particular, separate variations for each 2D ^{31}P REINE peak are obtained which reveal correlations between the *J* couplings and the ^{31}P chemical shifts of the coupled nuclei that are much clearer than those evident in previously presented 2D *z*-filtered ^{31}P spin−echo spectra. Notably, such correlations between the *J* couplings and the ^{31}P chemical shifts are observed even though the conditional probability distributions extracted using the protocol of Cadars et al. (*J. Am. Chem. Soc.* **2005**, *127*, 4466−4476) indicate that there is no marked correlation between the ^{31}P chemical shifts of neighboring phosphate tetrahedra. For 2D peaks at the P_2 ^{31}P chemical shift in the direct dimension, there can be contributions from chains of three units ($P_1-P_2-P_1$), chains of four units ($P_1-P_2-P_2-P_1$), or longer chains or rings ($-P_2-P_2-P_2-$): for the representative glass considered here, best fits are obtained assuming a glass comprised predominantly of chains of four units. The following variations are found: $^2J_{P_1,P_1} = 13.4 \pm 0.3$ to 14.8 ± 0.5 Hz, $^2J_{P_1,P_2} = 15.0 \pm 0.3$ to 18.2 ± 0.3 Hz, and $^2J_{P_2,P_2} = 5.9 \pm 0.6$ to 9.1 ± 0.9 Hz from the fits to the P_1-P_1, P_1-P_2, and P_2-P_2 peaks, respectively. The correlation of a particular *J* coupling with the ^{31}P chemical shifts of the considered nucleus and the coupled nucleus is quantified by the coefficients C_{F_2} and C_{F_1} that correspond to the average pixel-by-pixel change in the *J* coupling with respect to the chemical shift of the observed (F_2) and neighboring (F_1) ^{31}P nuclei, respectively.

1. Introduction

Glasses continue to find new technological applications; for example, multicomponent phosphate glasses are being developed for use in solid-state lasers,[1] as hosts for nuclear waste,[2] and in biomedical applications.[3−12] Various modern experimental techniques (e.g., X-ray and neutron diffraction, nuclear magnetic resonance (NMR), and vibrational spectroscopy) exist to characterize the microscopic- and atomic-scale structures that determine the bulk properties of a glass.[13] However, the insight provided is not sufficiently complete to provide an unrefutable description of glass structure, and there is considerable current and ongoing debate about even the simplest binary glass formers.[14−18] This debate is particularly centered on the presence or absence of so-called intermediate-range structure of glasses associated with the interconnection of adjacent structural units: is a disordered glass structure adequately described by Zachariasen's "random network" model,[18,19] or is there any ordering that reflects (if only partially) the regular structure of analogous

† Present address: Univ. Lyon, CNRS, ENS Lyon, UCB Lyon 1, Ctr RMN Très Hauts Champs, F-69100 Villeurbanne, France.

(1) Della Valle, G.; Festa, A.; Sorbello, G.; Ennser, K.; Cassagnetes, C.; Barbier, D.; Taccheo, S. *Opt. Express* **2008**, *16*, 12334–12341.
(2) Bingham, P. A.; Hand, R. J. *Mater. Res. Bull.* **2008**, *43*, 1679–1693.
(3) Knowles, J. C. *J. Mater. Chem.* **2003**, *13*, 2395–2401.
(4) Hertz, A.; Bruce, I. J. *Nanomedicine* **2007**, *2*, 899–918.
(5) Moss, R. M.; Pickup, D. M.; Ahmed, I.; Knowles, J. C.; Smith, M. E.; Newport, R. J. *Adv. Funct. Mater.* **2008**, *18*, 634–639.
(6) Qiu, D.; Guerry, P.; Ahmed, I.; Pickup, D. M.; Carta, D.; Knowles, J. C.; Smith, M. E.; Newport, R. J. *Mater. Chem. Phys.* **2008**, *111*, 455–462.
(7) Carta, D.; Qiu, D.; Guerry, P.; Ahmed, I.; Abou Neel, E. A.; Knowles, J. C.; Smith, M. E.; Newport, R. J. *J. Non-Cryst. Solids* **2008**, *354*, 3671–3677.
(8) Abou Neel, E. A.; O'Dell, L. A.; Smith, M. E.; Knowles, J. C. *J. Mater. Sci.: Mater. Med.* **2008**, *19*, 1669–1679.
(9) Pickup, D. M.; Abou Neel, E. A.; Moss, R. M.; Wetherall, K. M.; Guerry, P.; Smith, M. E.; Knowles, J. C.; Newport, R. J. *J. Mater. Sci.: Mater. Med.* **2008**, *19*, 1681–1685.
(10) Valappil, S. P.; Ready, D.; Abou Neel, E. A.; Pickup, D. M.; Chrzanowski, W.; O'Dell, L. A.; Newport, R. J.; Smith, M. E.; Wilson, M.; Knowles, J. C. *Adv. Funct. Mater.* **2008**, *18*, 732–741.
(11) O'Dell, L. A.; Abou Neel, E. A.; Knowles, J. C.; Smith, M. E. *Mater. Chem. Phys.* **2009**, *114*, 1008–1015.
(12) Carta, D.; Knowles, J. C.; Guerry, P.; Smith, M. E.; Newport, R. J. *J. Mater. Chem.* **2009**, *19*, 150–158.
(13) Greaves, G. N.; Sen, S. *Adv. Phys.* **2007**, *56*, 1–166.
(14) Salmon, P. S.; Martin, R. A.; Mason, P. E.; Cuello, G. J. *Nature* **2005**, *435*, 75–78.
(15) Umari, P.; Pasquarello, A. *Phys. Rev. Lett.* **2005**, *95*, 137401.
(16) Swenson, J.; Borjesson, L. *Phys. Rev. Lett.* **2006**, *96*, 199701.
(17) Ferlat, G.; Charpentier, T.; Seitsonen, A. P.; Takada, A.; Lazzeri, M.; Cormier, L.; Calas, G.; Mauri, F. *Phys. Rev. Lett.* **2008**, *101*, 065504.
(18) Wright, A. C. *Phys. Chem. Glass.* **2008**, *49*, 103–117.
(19) Zachariasen, W. H. *J. Am. Chem. Soc.* **1932**, *54*, 3841–3851.

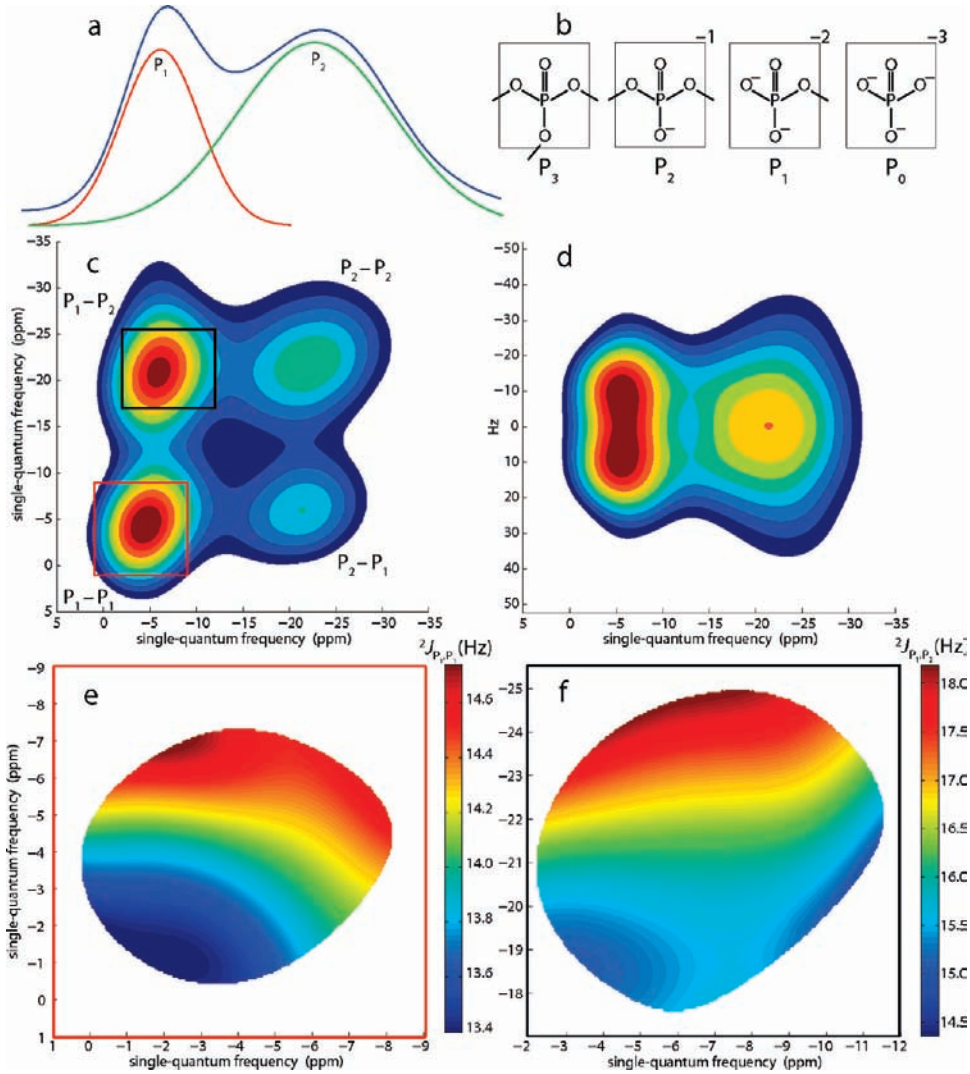

Figure 1. Extraction of structural information from ^{31}P (121.5 MHz) solid-state MAS NMR spectra of a cadmium phosphate glass. (a) A one-pulse spectrum allows the quantitative determination of the proportion of (b) P_n groups, whose relative proportions depend on the glass composition. (c) A 2D refocused INADEQUATE spectrum (in pseudo-COSY SQ−SQ representation) reveals the connectivity of P_n groups and (d) a 2D *z*-filtered spectrum partially resolves the $^2J_{P,P}$ coupling constants. (e) & (f) As described in this paper, the REINE experiment reveals 2D correlations of the *J* coupling strengths with the ^{31}P chemical shifts of the coupled nuclei.

crystalline phases? Such open questions motivate the development of novel analytical methodologies, with new experimental data being required to test and refine our understanding of glass structure; indeed, this is a prerequisite for identifying structure−function relationships that characterize the technologically important compositions.

NMR is sensitive to the local environment of the individual nuclear spins and is, thus, readily applicable to disordered solids that lack long-range periodic order.[20,21] For phosphate glasses, it is well established that the sensitivity of the NMR chemical shift to the local electronic environment enables, from a fitting of one-dimensional (1D) ^{31}P solid-state NMR spectra, the quantitative determination of the proportion of P_n groups, where *n* indicates the number of bridging oxygens.[22,23] This is illustrated in Figure 1a, which presents a ^{31}P MAS 1D spectrum of a representative phosphate glass. Moreover, the connectivity of P_n groups is revealed by 2D ^{31}P solid-state NMR spectra, which probe the through-space dipolar or through-bond *J* coupling between P_n groups: SQ (single-quantum)−SQ NOESY-like exchange spectra,[24−26] DQ (double-quantum)−SQ correlation spectra using dipolar recoupling,[25,27−32] and DQ−SQ[33,34]

(20) Schmidt-Rohr, K.; Spiess, H. W. *Multidimensional Solid-State NMR and Polymers*; Academic Press, 1994.
(21) Eckert, H.; Elbers, S.; Epping, J.; Janssen, M.; Kalwei, M.; Strojek, W.; Voigt, U. *New Technol. Solid State Nucl. Magn. Reson.* **2005**, *246*, 195–233.
(22) Eckert, H. *Prog. Nucl. Magn. Reson. Spectrosc.* **1992**, *24*, 159–293.
(23) Brow, R. K. *J. Non-Cryst. Solids* **2000**, *263&264*, 1–28.
(24) Jäger, C.; Feike, M.; Born, R.; Spiess, H. W. *J. Non-Cryst. Solids* **1994**, *180*, 91–95.
(25) Olsen, K. K.; Zwanziger, J. W.; Hartmann, P.; Jäger, C. *J. Non-Cryst. Solids* **1997**, *222*, 199–205.
(26) Alam, T. M.; Brow, R. K. *J. Non-Cryst. Solids* **1998**, *222*, 1–20.
(27) Feike, M.; Jäger, C.; Spiess, H. W. *J. Non-Cryst. Solids* **1998**, *223*, 200–206.
(28) Witter, R.; Hartmann, P.; Vogel, J.; Jäger, C. *Solid State Nucl. Magn. Reson.* **1998**, *13*, 189–200.
(29) Fayon, F.; Bessada, C.; Coutures, J. P.; Massiot, D. *Inorg. Chem.* **1999**, *38*, 5212–5218.
(30) Jäger, C.; Hartmann, P.; Witter, R.; Braun, M. *J. Non-Cryst. Solids* **2000**, *263&264*, 61–72.
(31) Tischendorf, B.; Otaigbe, J. U.; Wiench, J. W.; Pruski, M.; Sales, B. C. *J. Non-Cryst. Solids* **2001**, *282*, 147–158.

or TQ (triple-quantum)−SQ[35] *J* correlation spectra have been presented for various phosphate glasses. In the ^{31}P (DQ−SQ *J*) refocused INADEQUATE[33,36,37] spectrum in Figure 1c, P_1-P_1, P_1-P_2, P_2-P_1, and P_2-P_2 2D peaks are observed due to P_1-P_1, P_1-P_2, and P_2-P_2 connectivities of phosphate tetrahedra. The purpose of this paper is to demonstrate the wealth of structural information that can be extracted from the apparently featureless lineshapes in the refocused INADEQUATE spectrum of the representative amorphous phosphate glass (Figure 1c). The considered pulse sequence involves the appending of a spin−echo to the refocused INADEQUATE pulse sequence[38]—we refer to this as the *RE*focused *IN*ADEQUATE spin−*E*cho (REINE) experiment.

In solid-state NMR spectra, even under MAS, the observed line broadenings usually mask any underlying *J* splittings. This is particularly the case for disordered samples, where distributions of isotropic chemical shifts cause the free-induction-decay—the NMR signal arising from the direct detection of transverse magnetization—to be characterized by dephasing times, T_2^*, that are much shorter than the inverse of typically encountered *J* couplings. *J* couplings can, however, be quantitatively determined in solid-state MAS NMR spin−echo experiments.[34,38−63] This is because a spin−echo refocuses evolution under chemical shift offsets, such that for disordered samples the spin−echo dephasing time (T_2') is much longer than the decay time of the FID.[36,64−66] Importantly, Duma et al.[49] have demonstrated the robustness and accuracy of the simple spin−echo pulse sequence for measuring *J* coupling constants; indeed, it is found that the significantly larger chemical shift anisotropy (CSA) and dipolar interactions stabilize rather than perturb the measurement.

Two-dimensional *z*-filtered spin−echo ^{31}P MAS spectra have been presented for phosphate glasses.[34,52,59−61] As an example, such a 2D ^{31}P spin−echo spectrum of a lead phosphate glass, $0.66PbO-0.34P_2O_5$, shows a splitting due to a $^2J_{P,P}$ coupling for the broad P_1 resonance that increases from 17 to 20.5 Hz with decreasing ^{31}P chemical shift (increasing negative value).[34] A 2D ^{31}P MAS *z*-filtered spin−echo spectrum of the cadmium phosphate glass studied here is shown in Figure 1d. In this case, no chemical-shift-dependent change in the observed *J* splitting is evident. In contrast, this paper shows that the appending of a spin−echo to the refocused INADEQUATE pulse sequence in the REINE experiment reveals (respectively, shown in Figures 1e and 1f for the P_1-P_1 and P_1-P_2 2D peaks) the individual variations for the corresponding $^2J_{P,P}$ couplings. In this way, the REINE experiment unambiguously identifies differences in the *J* couplings between a P_1 and a P_2 unit ($^2J_{P_1,P_2}$) and those between two P_1 units ($^2J_{P_1,P_1}$) or two P_2 units ($^2J_{P_2,P_2}$). Importantly, the $^2J_{P,P}$ couplings are observed to be correlated with changes in the ^{31}P chemical shifts of the coupled nuclei. Specifically, considering any column in Figures 1e and 1f, the *J* couplings increase as the ^{31}P chemical shift of the coupled next-neighbor P_1 (see Figure 1e) or P_2 (see Figure 1f) nucleus becomes increasingly negative. Interestingly, there is a less evident change when considering rows in Figures 1e and 1f. This explains why no change is evident in the 2D ^{31}P MAS *z*-filtered spin−echo spectrum in Figure 1d. The observed variations in $^2J_{P,P}$ constitute a potentially rich new source of information for the characterization of so-called topological short-range order, namely, variations in bond angle and bond length.[67] Moreover, the fitting of the *J* modulation in the REINE spectra is shown (vide infra) to be sensitive to the chain lengths (in terms of connected polyhedra) in the glass.

2. Experimental Details

A phosphate glass of starting composition $0.575CdO-0.425P_2O_5$ was prepared as has been described by Hussin et al.[68] As noted in ref 68, the preparation in an alumina crucible leads to the incorporation of a small (<5%) proportion of Al_2O_3 into the glass.

(32) Fayon, F.; Massiot, D.; Suzuya, K.; Price, D. L. *J. Non-Cryst. Solids* **2001**, *283*, 88–94.
(33) Fayon, F.; Le Saout, G.; Emsley, L.; Massiot, D. *Chem. Commun.* **2002**, 1702–1703.
(34) Fayon, F.; King, I. J.; Harris, R. K.; Evans, J. S. O.; Massiot, D. *C. R. Chimie* **2004**, *7*, 351–361.
(35) Fayon, F.; Roiland, C.; Emsley, L.; Massiot, D. *J. Magn. Reson.* **2006**, *179*, 49–57.
(36) Lesage, A.; Bardet, M.; Emsley, L. *J. Am. Chem. Soc.* **1999**, *121*, 10987–10993.
(37) Fayon, F.; Massiot, D.; Levitt, M. H.; Titman, J. J.; Gregory, D. H.; Duma, L.; Emsley, L.; Brown, S. P. *J. Chem. Phys.* **2005**, *122*, 194393.
(38) Cadars, S.; Lesage, A.; Trierweiler, M.; Heux, L.; Emsley, L. *Phys. Chem. Chem. Phys.* **2007**, *9*, 92–103.
(39) Kubo, A.; McDowell, C. A. *J. Chem. Phys.* **1990**, *92*, 7156–7150.
(40) Challoner, R.; Nakai, T.; McDowell, C. A. *J. Chem. Phys.* **1991**, *94*, 7038–7045.
(41) Wu, G.; Wasylichen, R. E. *Inorg. Chem.* **1992**, *31*, 145–148.
(42) Eichele, K.; Wu, G.; Wasylishen, R. E. *J. Magn. Reson. A* **1993**, *101*, 157–161.
(43) Wu, G.; Wasylishen, R. E. *Inorg. Chem.* **1996**, *35*, 3113–3116.
(44) Brown, S. P.; Pérez-Torralba, M.; Sanz, D.; Claramunt, R. M.; Emsley, L. *Chem. Commun.* **2002**, 1852–1853.
(45) Fayon, F.; King, I. J.; Harris, R. K.; Gover, R. K. B.; Evans, J. S. O.; Massiot, D. *Chem. Mater.* **2003**, *15*, 2234–2239.
(46) Massiot, D.; Fayon, F.; Alonso, B.; Trebosc, J.; Amoureux, J.-P. *J. Magn. Reson.* **2003**, *164*, 160–164.
(47) Trebosc, J.; Amoureux, J.-P.; Delevoye, L.; Wiench, J. W.; Pruski, M. *Solid State Sci.* **2004**, *10*, 1089–1095.
(48) Eichele, K.; Nachtigal, C.; Jung, S.; Mayer, H. A.; Lindner, E.; Ströbele, M. *Magn. Reson. Chem.* **2004**, *42*, 807–813.
(49) Duma, L.; Lai, W.; Carravetta, M.; Emsley, L.; Brown, S. P.; Levitt, M. H. *ChemPhysChem* **2004**, *5*, 815–833.
(50) Brown, S. P.; Emsley, L. *J. Magn. Reson.* **2004**, *171*, 43–47.
(51) Amoureux, J.; Trebosc, J.; Wiench, J.; Massiot, D.; Pruski, M. *Solid State Nucl. Magn. Reson.* **2005**, *27*, 228–232.
(52) de Araujo, C. C.; Strojek, W.; Zhang, L.; Eckert, H.; Poirier, G.; Ribeirob, S. J. L.; Messaddeq, Y. *J. Mater. Chem.* **2006**, *16*, 3277–3284.
(53) Foucault, H. M.; Bryce, D. L.; Fogg, D. E. *Inorg. Chem.* **2006**, *45*, 10293–10299.
(54) Montouillout, V.; Morais, C. M.; Douy, A.; Fayon, F.; Massiot, D. *Magn. Reson. Chem.* **2006**, *44*, 770–775.
(55) Lai, W.; et al. *J. Am. Chem. Soc.* **2006**, *128*, 3878–3879.
(56) Cadars, S.; Lesage, A.; Hedin, N.; Chmelka, B. F.; Emsley, L. *J. Phys. Chem. B* **2006**, *110*, 16982–16991.
(57) Pham, T. N.; Griffin, J. M.; Masiero, S.; Lena, S.; Gottarelli, G.; Hodgkinson, P.; Filip, C.; Brown, S. P. *Phys. Chem. Chem. Phys.* **2007**, *9*, 3416–3423.
(58) Martineau, C.; Fayon, F.; Legein, C.; Buzare, J.-Y.; Silly, G.; Massiot, D. *Chem. Commun.* **2007**, *26*, 2720–2722.
(59) Rinke, M. T.; Zhang, L.; Eckert, H. *ChemPhysChem* **2007**, *8*, 1988–1998.
(60) van Wullen, L.; Tricot, G.; Wegner, S. *Solid State Nucl. Magn. Reson.* **2007**, *32*, 44–52.
(61) Wegner, S.; van Wullen, L.; Tricot, G. *J. Non-Cryst. Solids* **2008**, *354*, 1703–1714.
(62) Florian, P.; Fayon, F.; Massiot, D. *J. Phys. Chem. C* **2009**, *113*, 2562–2572.
(63) Hung, I.; Uldry, A.-C.; Becker-Baldus, J.; Webber, A. L.; Wong, A.; Smith, M. E.; Joyce, S. A.; Yates, J.; Pickard, C. J.; Dupree, R.; Brown, S. P. *J. Am. Chem. Soc.* **2009**, *131*, 1820–1834.
(64) Cowans, B. A.; Grutzner, J. B. *J. Magn. Reson. A* **1993**, *105*, 10–18.
(65) de Paëpe, G.; Giraud, N.; Lesage, A.; Hodgkinson, P.; Böckmann, A.; Emsley, L. *J. Am. Chem. Soc.* **2003**, *125*, 13938–13939.
(66) Hodgkinson, P. *Prog. Nucl. Magn. Reson. Spectrosc.* **2005**, *46*, 197–222.

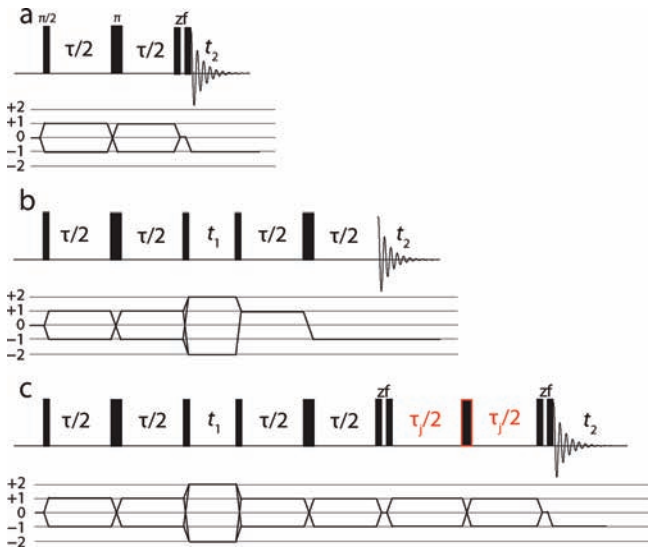

Figure 2. Pulse sequence and corresponding coherence transfer pathway diagram for (a) the *z*-filtered spin−echo, (b) the refocused INADEQUATE,[33,36,37] and (c) the refocused INADEQUATE spin−echo[38] (REINE) experiments. Thin and thick rectangles, respectively, represent $\pi/2$ and π pulses. The additional spin−echo period, τ_j, in the (c) REINE experiment, which allows the detection of the *J* modulation for each 2D peak, is highlighted in red.

Experiments were performed on a Varian 7.05 T magnetic field Infinity$^+$ spectrometer, corresponding to a ^{31}P Larmor frequency of 121.5 MHz, using a Bruker 4 mm MAS probe. The spectral widths in the F_1 (except for the *z*-filtered spin−echo experiment) and F_2 dimensions were set equal to the MAS frequency of 12.5 kHz. The ^{31}P $\pi/2$ pulse duration was 3 μs. A recycle delay of 24 s (14 s for the *z*-filtered spin−echo experiment) was inserted between a comb of saturation pulses and the first $\pi/2$ pulse. Spectra were referenced to the resonance of ammonium dihydrogen phosphate ($NH_4H_2PO_4$) at 0.9 ppm.[69]

The pulse sequences and coherence transfer pathway diagrams for the *z*-filtered spin−echo, refocused INADEQUATE,[33,36,37] and REfocused INadequate spin−Echo (REINE)[38] experiments are shown in Figure 2. For the *z*-filtered spin−echo experiment, 32 transients were coadded for each of the 20 t_1 increments of 2.4 ms. Otherwise, 64 (refocused INADEQUATE) and 320 (REINE) transients were coadded for each of the 18 t_1 slices. Quadrature detection in t_1 was achieved by using the States−Haberkorn−Ruben method.[70] REINE spectra were recorded for 11 increasing spin−echo delays. The *z*-filter delays were of 4 ms duration, and no difference in signal intensity was noticed on increasing these to 50 ms. Phase-cycling schemes of 16, 16, and 32 steps were employed for the *z*-filtered spin−echo, refocused INADEQUATE, and REINE sequences, respectively. For the *z*-filtered spin−echo experiments, a four-step cycle of the π pulse (to select $\Delta p = -2$, where *p* is the coherence order) was nested with a four-step cycle of the z-filter; for the refocused INADEQUATE experiment, nested four-step phase cycles were used to select $\Delta p = \pm 2$ for the first three pulses—as a block—and the first π pulse; for the REINE experiment, a four-step phase cycle of the first three pulses—as a block—(to select $\Delta p = \pm 2$) was nested with a two-step phase cycle of the second π pulse (pulse phase 0, π; receiver phase 0, π) and a four-step phase cycle of the final *z*-filter. *J* couplings and spin−echo dephasing times were obtained by fitting the time-domain spin−echo evolution curves of each pixel in the REINE spectra for which the signal at $\tau_j = 0$ exceeded 66% of the individual maximum peak intensity for the P_1-P_1 and P_1-P_2 peaks and exceeded 75% for the P_2-P_1 and P_2-P_2 peaks. This corresponded to 15 565, 18 808, 15 430, and 20 977 individual fittings for the P_1-P_1, P_1-P_2, P_2-P_1, and P_2-P_2 REINE peaks, respectively, where there were 10 pixels per parts per million in both dimensions. Errors and correlation coefficients were calculated from the covariance matrix as described by Pham et al.[57]

3. One-Dimensional and Two-Dimensional Refocused INADEQUATE ^{31}P NMR: Identification of the Number of Bridging Oxygens and Next-Nearest-Neighbor Connectivity of Phosphate Units

Phosphate glasses are structured around PO_4 units, linked by bridging oxygens to form various phosphate anions (see Figure 1b).[23,71] The P_n terminology is traditionally used,[72] with *n* indicating the number of bridging oxygens per tetrahedron, to distinguish groups with different degrees of connectivity to other phosphate units. Vitreous P_2O_5 is composed exclusively of cross-linking P_3 tetrahedra. However, depolymerization of the glass network and the formation of P_2, P_1, and P_0 units is achieved through the inclusion of network-modifying cations (Na^+, Ca^{2+}, Cd^{2+}, etc.) in varying concentrations, the lesser connected phosphate anions requiring a greater number of cations to maintain charge balance.

One-dimensional ^{31}P MAS NMR spectra identify the P_n groups on the basis of their respective chemical shifts,[23] as shown in Figure 1a for the cadmium phosphate glass. Specifically, the broad high- and low-frequency resonances are assigned to P_1 and P_2 groups, respectively. For the cadmium phosphate glass of nominal composition $0.575CdO-0.425P_2O_5$ studied here, the fitting of the 1D MAS NMR spectrum in Figure 1a yields a proportion of 58 ± 5% of the phosphate tetrahedra having two bridging oxygens, whereas the remaining 43 ± 5% have only one. These results can be compared with, on the one hand, the well-established chemical-ordering (binary) model[23,71] for the structure of phosphate glasses—which for a polyphosphate glass, $xRO(1-x)P_2O_5$, where $0.50 < x < 0.67$, predicts $(2x-1)/(1-x) = 35.3\%$ and $(2-3x)/(1-x) = 64.7\%$ of P_1 and P_2 units, respectively—and, on the other hand, those from a previous study on a range of cadmium phosphate glasses.[68]

A ^{31}P refocused INADEQUATE 2D spectrum of the cadmium phosphate glass is shown in Figure 1c. The spectrum is shown in a pseudo-COSY SQ−SQ representation.[45] Linkages between like units are therefore evidenced by peaks on the diagonal, whereas correlations between units with different isotropic chemical shifts appear on either side of the diagonal. In Figure 1c, P_1-P_1, P_1-P_2, P_2-P_1, and P_2-P_2 2D DQ peaks are observed due to P_1-P_1, P_1-P_2, and P_2-P_2 connectivities of phosphate tetrahedra. To discuss the interconnectivity of the phosphate tetrahedra, the notation $P_n^{j,k,l}$ is introduced where $n = 0,1,2,3$ indicates the number of bridging oxygens for a particular unit, and the connectivity of each neighboring phosphate is indicated by *n* separate indices *j*,*k*,*l*.[28] It is evident that the P_1-P_1 and P_1-P_2 2D DQ peaks as well as the P_2-P_1 and P_2-P_2 2D DQ peaks in Figure 1c are centered at different ^{31}P SQ frequencies—this has been noted previously for 2D ^{31}P DQ MAS spectra of

(67) Lee, S. K.; Musgrave, C. B.; Zhao, P. D.; Stebbins, J. F. *J. Phys. Chem. B* **2001**, *105*, 12583–12595.
(68) Hussin, R.; Holland, D.; Dupree, R. *J. Non-Cryst. Solids* **2002**, *298*, 32–42.
(69) MacKenzie, K. J. D.; Smith, M. E. *Multinuclear Solid State NMR of Inorganic Materials*; Pergamon, 2002.
(70) States, D. J.; Haberkorn, R. A.; Ruben, D. J. *J. Magn. Reson.* **1982**, *48*, 286–292.
(71) van Wazer, J. R. *Phosphorus and Its Compounds*; Interscience, 1958; Vol. 1.
(72) Liebau, F. *Structure and Bonding in Crystals*; Academic Press, New-York, 1981; Vol. 2, p 197.

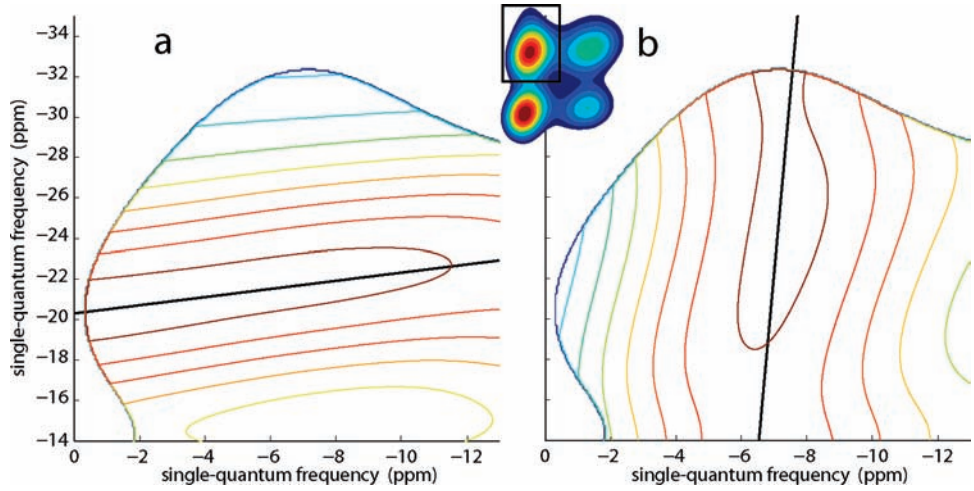

Figure 3. Chemical-shift correlations as determined from a ^{31}P (121.5 MHz) MAS NMR refocused INADEQUATE spectrum (in pseudo-COSY representation, see Figure 1c) of a cadmium phosphate glass using the procedure described by Cadars et al.[73] (a) M_1 and (b) M_2 conditional probability matrices for P_1 units bonded to P_2 tetrahedra; a point in (a), $M_1(\omega^i_{P_2},\omega^k_{P_1})$, corresponds to the probability, for the P_1-P_2 dimers, that the P_2 unit has a chemical shift $\omega^i_{P_2}$ given that the P_1 tetrahedron it is coupled to resonates at $\omega^k_{P_1}$. Similarly, a point in (b), $M_2(\omega^i_{P_2},\omega^k_{P_1})$, corresponds to the probability that the P_1 tetrahedron has a chemical shift $\omega^k_{P_1}$ given that the P_2 unit it is coupled to resonates at $\omega^i_{P_2}$. The probability contours indicate that there is no propensity for P_1 tetrahedra to be linked to P_2 units of a particular chemical shift. The black lines correspond to the slopes c^1_{ki} and c^2_{ki}, obtained by fitting the position of maximum intensity of each row or column to straight lines. (Note that a normalization procedure is first applied whereby the sum of intensities in either each column or row in the considered region of the pseudo-COSY spectrum is set equal to unity.) The contour levels are given by ([minimum,maximum] $\times 10^{-3}$) (a) [20, 55] and (b) [20, 50].

other phosphate glasses.[27−30,32,34] Indeed, it has been shown that the chemical shifts for distinct $P_n^{j,k,l}$ phosphate units, as determined from the position of 2D peaks, can be used as fixed parameters in multipeak fits of one-dimensional ^{31}P spectra, to quantify the proportion of the different phosphate units.[28−30,34]

In principle, the information content of refocused INADEQUATE spectra is not limited to the mere observation of 2D correlation peaks that identify specific next-nearest neighbors. Importantly, for sequences built around spin−echo blocks, the spectral resolution is governed by the spin−echo dephasing time, T_2'.[36,73] As noted above, for disordered samples such as amorphous glasses, T_2' can be orders of magnitude longer than the FID decay constant, T_2^*: for the cadmium phosphate glass investigated here, T_2' (≃35 ms) is approximately 175 times longer than T_2^* (≃0.2 ms). Recently, Cadars et al.[73] have presented a procedure by which chemical-shift correlations can be extracted from 2D refocused INADEQUATE spectra. Such chemical-shift correlations reflect the near intermediate-range order (neighboring phosphate unit, i.e., 3−4 Å for phosphate glasses)[74] in the sample (or lack thereof), by indicating the probability that there is a through-bond J coupling between two structural units with specific chemical shifts.

The conditional probability matrices extracted from the P_1-P_2 peak of the pseudo-COSY spectrum for the cadmium phosphate glass are presented in Figure 3 (similar profiles are obtained for the three other correlation peaks, see Supporting Information). Two maps are obtained for the (single) P_1-P_2 peak that correspond to (Figure 3a) the conditional probability that the P_2 unit has a chemical shift $\omega^i_{P_2}$ given that the P_1 tetrahedron it is coupled to resonates at $\omega^k_{P_1}$ and (Figure 3b) the conditional probability that the P_1 tetrahedron has a chemical shift $\omega^k_{P_1}$ given that the P_2 unit it is coupled to resonates at $\omega^i_{P_2}$. (Note that a normalization procedure is first applied whereby the sum of intensities in either each column or row in the considered region of the pseudo-COSY spectrum is set equal to unity.) The two different conditional probability matrices differ only in the information that is considered known. In Figure 3a, the contours are approximately horizontal: this means that the conditional probability of the ^{31}P chemical shift of a P_2 unit being, say, −22 ppm is approximately the same regardless of the ^{31}P chemical shift of the coupled P_1 unit. In Figure 3b, the contours are approximately vertical: this means that the conditional probability of the ^{31}P chemical shift of a P_1 unit being, say, −7 ppm is approximately the same regardless of the ^{31}P chemical shift of the coupled P_2 unit. Such approximately horizontal and vertical contours thus indicate the absence of any marked correlation. This is different from conditional probability matrices that exhibit evident slopes—indicative of a correlation between the chemical shifts of the coupled nuclei—that have been presented previously for ^{13}C, ^{29}Si, and ^{31}P refocused INADEQUATE spectra of a cellulose sample extracted from wood,[73] surfactant-templated silicate layers,[75] and a diphenylphosphino amine,[73,76] respectively.

Recently, Cadars et al.[75,76] have shown that the degree of correlation can be quantified by either the degree of chemical shift correlation, r_{ki},[75] or a Pearson product-moment coefficient, ρ_{ki}.[77] Table 1 lists the correlation coefficients as extracted for the P_1-P_1, P_1-P_2, P_2-P_1, and P_2-P_2 2D peaks. Both correlation coefficients can vary between 0 and 1, and the low values are again indicative of the absence of any clear correlation between the chemical shifts of the coupled nuclei. (For all four peaks, the Pearson coefficient is the smaller of the two, as has been previously noted in ref 76.)

(73) Cadars, S.; Lesage, A.; Emsley, L. *J. Am. Chem. Soc.* **2005**, *127*, 4466–4476.
(74) Hoppe, U.; Walter, G.; Kranold, R.; Stachel, D. *J. Non-Cryst. Solids* **2000**, *263 & 264*, 29–47.
(75) Cadars, S.; Mifsud, N.; Lesage, A.; Epping, J. D.; Hedin, N.; Chmelka, B. F.; Emsley, L. *J. Phys. Chem. C* **2008**, *112*, 9145–9154.
(76) Cadars, S.; Lesage, A.; Pickard, C. J.; Sautet, P.; Emsley, L. *J. Phys. Chem. A* **2009**, *113*, 902–911.
(77) Cohen, J.; West, S. G.; Cohen, P.; Aiken, L. S. *Applied multiple regression/correlation analysis for the behavioral sciences*; Lawrence Erlbaum Assoc. Inc.: Hillsdale, NJ, 2003.

Table 1. Chemical-Shift Correlation Coefficients for the 2D Refocused INADEQUATE Peaks

peak[a]	r_{ki}	ρ_{ki}
P_1-P_1	0.21	0.18
P_1-P_2	0.11	0.07
P_2-P_1	0.16	0.09
P_2-P_2	0.23	0.12

[a] Regions ([max,min] in ppm) over which the analysis was performed for the refocused INADEQUATE spectrum (in a pseudo-COSY SQ−SQ representation) as shown in Figure 1c. P_1-P_1, F_1 and F_2: [3, −12]; P_1-P_2, F_1: [−14, −35], F_2: [0, −13]; P_2-P_1, F_1: [0, −12], F_2: [−14, −29]; P_2-P_2, F_1 and F_2: [−16, −32].

Table 2. Spin−Echo Modulations Arising for Different Phosphate Chain Lengths

chain	length	units[a]	*J* modulation[b]
P_1-P_1	2	$2 \times n_2 \times P_1^1$	cos(11)
$P_1-P_2-P_1$	3	$2 \times n_3 \times P_1^2$	cos(12)
		$n_3 \times P_2^{1,1}$	$\cos^2(12)$
$P_1-P_2-P_2-P_1$	4	$2 \times n_4 \times P_1^2$	cos(12)
		$2 \times n_4 \times P_2^{1,2}$	cos(12) × cos(22)
$P_1-P_2(-P_2)_m-P_2-P_1$	$l \geq 5$	$2 \times n_l \times P_1^2$	cos(12)
		$2 \times n_l \times P_2^{1,2}$	cos(12) × cos(22)
		$(l-4) \times n_l \times P_2^{2,2}$	$\cos^2(22)$
$(-P_2-)_r$	r	$n_{R_r} \times r \times P_2^{2,2}$	$\cos^2(22)$

[a] The proportion of phosphate chains of length l is denoted n_l, while n_{R_r} denotes the proportion of phosphate rings made up of r units. [b] $\cos(ij) = \cos(\pi[^2J_{P_i,P_j}]\tau_j)$.

In conclusion, the conditional probability matrix analysis indicates that a P_1 unit resonating at a particular chemical shift has an equal probability of being linked to any of the P_2 tetrahedra and vice versa and similarly for the P_1-P_1 and P_2-P_2 connectivities. Specifically, the number of P_1-O-P_2 bonds with a particular conformation is entirely governed by the Gaussian distributions of P_1 and P_2 local environments as evidenced in the 1D MAS spectrum (Figure 1a). Thus, the analysis here suggests that the linear chains in this sample are assembled randomly and that there is no marked preferential order in these structures beyond the first oxygen bond.

4. Two-Dimensional ^{31}P NMR REINE Experiments: Phosphate Chain Lengths

The assignment of the 2D correlation peaks at the P_1 SQ frequency in Figure 1c to either P_1^1 or P_1^2 units is simple and unambiguous. By contrast, in a glass, chains of different length can contribute to the 2D correlation peaks at the P_2 SQ frequency.[28] In this section, it is shown that valuable information about the chain-length distribution is encoded into the *J* coupling evolution that occurs during the final spin−echo of the REINE[38] experiment (see Figure 2c).

Table 2 shows the distinct spin−echo modulations associated with different chain lengths of linked phosphate tetrahedra in a glass. In principle, it is possible therefore to identify the presence of different chain lengths from ^{31}P spin−echo experiments. However, in a spin−echo experiment, a superposition of different modulations will usually preclude a reliable fitting; e.g., for a P_1 resonance, there can be contributions from P_1-P_1 and P_1-P_2 connectivities, with the $^2J_{P_1,P_1}$ and $^2J_{P_1,P_2}$ couplings likely to be of different magnitude.

In the refocused INADEQUATE experiment[36,37] (see Figure 2b), *J* couplings are used to create double-quantum coherences, but the intensity of the 2D correlation peaks has a complicated dependence on the spin−echo duration, τ, for the case of three or more coupled nuclei.[78] In the REINE experiment,[38] a third spin−echo is appended to the refocused INADEQUATE pulse sequence, allowing the recording of the distinct spin−echo modulation under the *J* coupling(s) for the separate 2D correlation peaks.

Table 3. *J* Modulations of the 2D Peaks in REINE Spectra for the Possible Lengths of Phosphate Chains

REINE peak	*J* modulation[a,b]
P_1-P_1	cos(11)
P_1-P_2	cos(12)
P_2-P_1	$n_3 \times \cos^2(12) + 2 \times (n_4 + n_{5+}) \times \cos(12) \times \cos(22)$
P_2-P_2	$2 \times (n_4 + n_{5+}) \times \cos(12) \times \cos(22) + (\sum_{l=5}^{\infty}(l-4) \times n_l + \sum_{r=3}^{\infty} r \times n_{R_r}) \times \cos^2(22)$

[a] The proportion of phosphate chains of length l is denoted n_l, while n_{R_r} denotes the proportion of phosphate rings made up of r units (see Table 2). [b] $\cos(ij) = \cos(\pi[^2J_{P_i,P_j}]\tau_j)$.

Table 3 lists the *J* modulations associated with the different phosphate chain lengths that can contribute to the four distinct REINE peaks observed for the cadmium phosphate glass (see Figure 1c). For the REINE peaks at the P_1 frequency in F_2 (P_1-P_1 and P_1-P_2), a single cosine modulation due to their evolution under a single *J* coupling is qualitatively—but not quantitatively (since $^2J_{P_1,P_1}$ and $^2J_{P_1,P_2}$ are likely to have different magnitudes)—the same for all chain lengths. The situation is more complicated for the REINE peaks at the P_2 frequency in F_2 (P_2-P_1 and P_2-P_2), since Table 3 reveals that the observed modulation depends on the chain-length distribution if $^2J_{P_1,P_2}$ is not equal to $^2J_{P_2,P_2}$. For example, if the glass structure is composed mainly of long chains or P_2 rings, the $\cos^2(\pi[^2J_{P_2,P_2}]\tau_j)$ modulation of $P_2^{2,2}$ units dominates for the P_2-P_2 correlation peak, whereas if there are predominately chains of four units present, the P_2-P_2 peak will exhibit the $\cos(\pi[^2J_{P_2,P_2}]\tau_j) \times \cos(\pi[^2J_{P_1,P_2}]\tau_j)$ modulation from the $P_2^{1,2}$ tetrahedra. Note that for this case of chains of four units, $P_1-P_2-P_2-P_1$, both REINE peaks at the P_2 SQ frequency (P_2-P_1 and P_2-P_2) exhibit identical *J* modulations, since both $P_2^{1,2}$ tetrahedra in the chains are linked to one P_1 and one P_2 group.

When fitting the spin−echo curves for the four REINE peaks, it follows from Table 3 that different fitting equations are appropriate for the spin−echo curves both for the case of the distinct REINE peaks and also for different chain-length distributions. For the P_1-P_1 and P_1-P_2 REINE peaks, the fitting function is a damped single-cosine modulation

$$I(\tau_j) = I_0 \times \cos(\pi J \tau_j) \times e^{(-\tau_j/T_2')} \quad (1)$$

since by definition P_1 units are only *J*-coupled to one other phosphate group. (The spin−echo fitting function in eq 78 of Duma et al.[49] includes an additional term that considers a proportion with only a $e^{(-\tau_j/T_2')}$ modulation. As described in the Supporting Information, fittings of REINE data to such a function returned negligible proportions for this additional zero-frequency term, and hence the simplified expression in eq 1 was used.) For the REINE peaks at the P_2 SQ frequency, evolution can occur under the $^2J_{P_1,P_2}$ and/or $^2J_{P_2,P_2}$ couplings, with three fitting functions being applicable depending on the chain-length distribution

$$I(\tau_j) = I_0 \times \cos(\pi J_1 \tau_j)\cos(\pi J_2 \tau_j) \times e^{(-\tau_j/T_2')} \quad (2)$$

(78) Cadars, S.; Sein, J.; Duma, L.; Lesage, A.; Pham, T. N.; Baltisberger, J. H.; Brown, S. P.; Emsley, L. *J. Magn. Reson.* **2007**, *188*, 24–34.

$$I(\tau_j) = I_0 \times \cos^2(\pi J \tau_j) \times e^{(-\tau_j/T_2')} \quad (3)$$

$$I(\tau_j) = I_0(p\cos^2(\pi J_2 \tau_j) + (1-p)\cos(\pi J_1 \tau_j)\cos(\pi J_2 \tau_j))e^{(-\tau_j/T_2')} \quad (4)$$

Equation 2 is applicable for the P_2-P_1 peak if there is a negligible proportion of triphosphate chains (i.e., $n_3 = 0$) and for the P_2-P_2 peak for the case of tetraphosphate chains. Equation 3 characterizes the modulation for the P_2-P_1 peak if there are only triphosphate chains present—in which case $J = {}^2J_{P_1,P_2}$—and that for the P_2-P_2 peak if long phosphate chains or rings are predominant—in which case $J = {}^2J_{P_2,P_2}$. Equation 4 is a combination of the two preceding functions where $0 \le p \le 1$ is the proportion of units with a $\cos^2$ modulation; for the P_2-P_1 peak, where $J_1 = {}^2J_{P_2,P_2}$ and $J_2 = {}^2J_{P_1,P_2}$, it is applicable where short (three units), medium (four or five units), and long (six or more units) linear chains and/or phosphate rings coexist; for the P_2-P_2 peak, where $J_1 = {}^2J_{P_1,P_2}$ and $J_2 = {}^2J_{P_2,P_2}$, eq 4 is applicable where medium (four or five units) and long (six or more units) linear chains and/or phosphate rings coexist.

In this section, single time-domain spin−echo curves are fitted for each of the four 2D REINE peaks; i.e., each curve corresponds to the modulation of the total intensity summed across each REINE peak. The four summed spin−echo curves for the cadmium phosphate glass are presented in Figure 4, along with (as insets) the Fourier transforms of the best-fit functions. The fit parameters and correlation coefficients are given in Table 4. Note that this technique allows the separate measurement of the ${}^2\bar{J}_{P_1,P_1}$ (14.0 ± 0.4 Hz, Figure 4a) and ${}^2\bar{J}_{P_1,P_2}$ (16.3 ± 0.4 Hz, Figure 4c) average couplings, from the best fits for the P_1-P_1 and P_1-P_2 REINE peaks to eq 1. The determination of a significant difference between ${}^2\bar{J}_{P_1,P_1}$ and ${}^2\bar{J}_{P_1,P_2}$ highlights the advantage of the REINE sequence over the spin−echo sequence on its own; in the latter, the observed modulation would be a superposition of that due to P_1^1 and P_1^2 groups.

Table 4. Fitting Results for the Time-Domain REINE Curves

peak	equation	ε^{2a}	fitted parameters (${}^2\bar{J}_{P,P}$ in Hz; T_2' in ms)	correlation coefficient(s)
P_1-P_1	1	4.1×10^{-3}	${}^2\bar{J}_{P_1,P_1} = 14.0 \pm 0.4$ $T_2' = 38.7 \pm 1.6$	${}^2\bar{J}_{P_1,P_1}-T_2'$: 0.01
P_1-P_2	1	6.3×10^{-3}	${}^2\bar{J}_{P_1,P_2} = 16.3 \pm 0.4$ $T_2' = 36.5 \pm 1.7$	${}^2\bar{J}_{P_1,P_2}-T_2'$: 0.15
P_2-P_1	2	4.7×10^{-3}	${}^2\bar{J}_{P_1,P_2} = 13.5 \pm 0.8$ ${}^2\bar{J}_{P_2,P_2} = 7.7 \pm 0.6$ $T_2' = 33.0 \pm 3.6$	${}^2\bar{J}_{P_1,P_2}-T_2'$: 0.62 ${}^2\bar{J}_{P_2,P_2}-{}^2\bar{J}_{P_1,P_2}$: 0.00 ${}^2\bar{J}_{P_2,P_2}-T_2'$: 0.18
P_2-P_2	2	1.5×10^{-3}	${}^2\bar{J}_{P_1,P_2} = 14.3 \pm 0.4$ ${}^2\bar{J}_{P_2,P_2} = 7.4 \pm 0.3$ $T_2' = 31.9 \pm 2.0$	${}^2\bar{J}_{P_1,P_2}-T_2'$: 0.57 ${}^2\bar{J}_{P_2,P_2}-{}^2\bar{J}_{P_1,P_2}$: 0.15 ${}^2\bar{J}_{P_2,P_2}-T_2'$: 0.35

[a] $\varepsilon^2 = \Sigma_n(I_n^{fit} - I_n^{experiment})^2/\Sigma_n(I_n^{experiment})^2$.

The spin−echo modulations for the two REINE peaks at the P_2 frequency in F_2 (P_2-P_1 and P_2-P_2) are shown in Figures 4b and 4d. For both cases, an accurate fit with physically reasonable values and acceptable correlation coefficients was only achieved for eq 2 (see Supporting Information for fits to the other equations). The fitted average J couplings are: ${}^2\bar{J}_{P_1,P_2} = 13.5 \pm 0.8$ Hz, ${}^2\bar{J}_{P_2,P_2} = 7.7 \pm 0.6$ Hz and ${}^2\bar{J}_{P_1,P_2} = 14.3 \pm 0.4$ Hz, ${}^2\bar{J}_{P_2,P_2} = 7.4 \pm 0.3$ Hz, respectively, for the P_2-P_1 and P_2-P_2 peaks. The fact that the average spin−echo modulations for the two REINE peaks are the same, qualitatively and quantitatively, is consistent with the P_2 units in this sample being predominantly

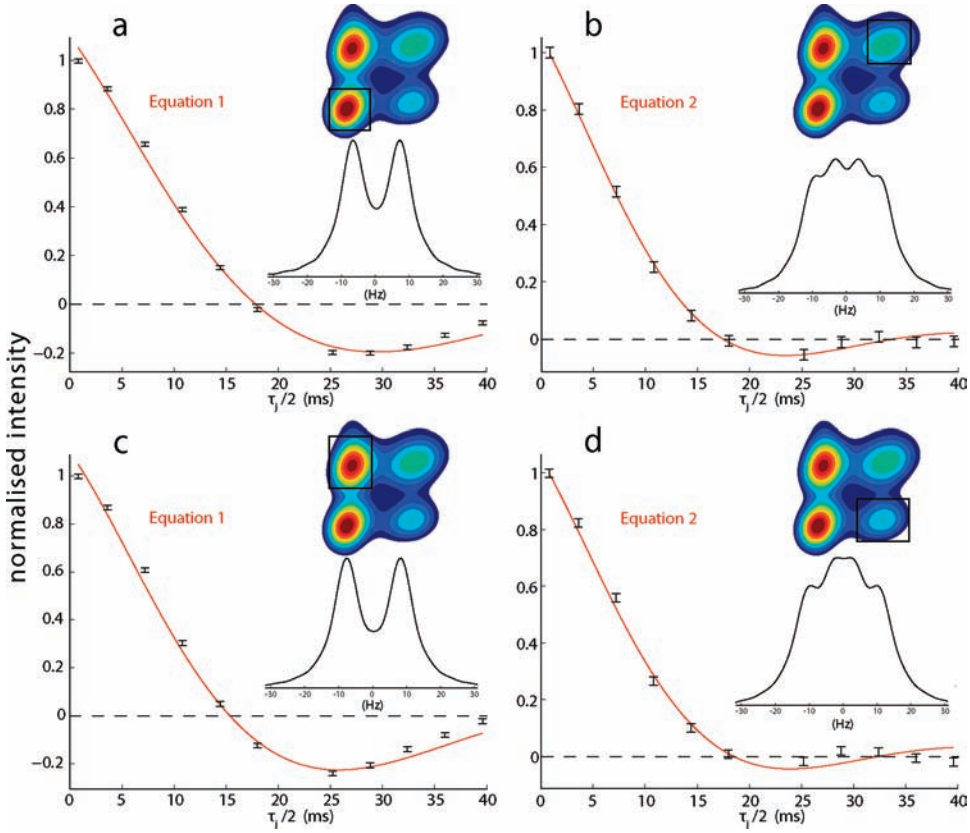

Figure 4. Time-domain spin−echo curves as obtained from ^{31}P (121.5 MHz) MAS NMR REINE spectra (in pseudo-COSY representation) of the cadmium phosphate glass. Modulation of the summed intensity, respectively, across the (a) P_1-P_1, (b) P_2-P_2, (c) P_1-P_2, and (d) P_2-P_1 refocused INADEQUATE peaks as a function of the τ_j echo delay. Best fits to eq 1 ((a) and (c)) and eq 2 ((b) and (d)) are shown as solid red lines—the fit parameters and correlation coefficients are given in Table 4. The Fourier transforms of the best-fit functions are shown as insets.

in chains of four tetrahedra. Together with the intense P_1-P_1 peak in the refocused INADEQUATE spectrum, this analysis of the *average* coupling constants suggests a glass composed mainly of phosphate dimers and short tetraphosphate chains.

Specific aspects of the fits presented above need careful explanation. First, the P_1-P_1 and P_2-P_2 2D peaks correspond to cases where the ^{31}P isotropic chemical shifts of the coupled nuclei are the same or very similar. In solution-state NMR, no *J* modulation is seen for such cases where the isotropic chemical shifts of the coupled nuclei are identical. However, the situation in solid-state NMR is different because of the CSA: as described in ref 49, a *J* modulation is observed for the case of two coupled nuclei with identical isotropic chemical shifts (this is referred to as $n = 0$ rotational resonance) and identical chemical shift anisotropy and asymmetry parameters provided that the orientations of the two CSA tensors are different. (This is demonstrated, in the Supporting Information, by the fitting of REINE spin−echo data, simulated for ^{31}P nuclei and the experimental parameters.)

It is to be further noted that Fayon et al. have presented a combined analytical, numerical simulation, and experimental analysis of the excitation and reconversion of DQ coherence in the refocused INADEQUATE experiment for two coupled spin-1/2 nuclei.[37] Specifically, for the case of $n = 0$ rotational resonance where there is both a *J* and a dipolar coupling, the intensity build-up (as a function of the refocused INADEQUATE spin−echo durations) exhibits a complex behavior, from which neither the *J* nor the dipolar coupling can be extracted without a detailed prior knowledge of the spin system. In this work, it is to be emphasized that in the REINE experiment it is the simpler *J* modulation in the additional appended spin−echo (highlighted in red in Figure 2c) that is monitored.

For the fits in this section of the spin−echo modulation for the summed intensity across each of the REINE 2D peaks, it is additionally necessary to consider the damping effect of a *J* distribution on the observed spin−echo *J* modulation. This effect is illustrated in Figure 1 of ref 38, which presents spin−echo modulation curves simulated for an ensemble of isolated pairs of *J*-coupled nuclei with a Gaussian distribution of *J* couplings; for a mean *J* coupling of 50 Hz and a T_2' decay time of 100 ms, the effect of increasing the standard deviation of the Gaussian distribution from 0 to 20 Hz led to a marked damping of the total summed spin−echo modulation. This causes a small deviation in the fitted *J* coupling away from the mean value together with a marked drop in the fitted dephasing time as compared to the actual value for each individual spin−echo curve. In the Supporting Information of this paper, analogous simulations are presented for a mean *J* coupling of 16 Hz and a T_2' decay time of 35 ms, corresponding to the fitted values in Table 4 for the P_1-P_2 REINE peak. It is seen that an evident damping that causes a significant change in the fitted dephasing time is only evident for a standard deviation of the Gaussian distribution of 4 Hz or more. In this context, the pixel-by-pixel fits presented in the next section show no more than a $\pm$ 2 Hz variation in *J* coupling, indicating that the extracted dephasing times presented in Table 4 are reliable measures of the true individual T_2' times.

5. Two-Dimensional ^{31}P NMR REINE Experiments: Correlations of $^2J_{P,P}$ Couplings with ^{31}P Chemical Shifts

The above section presented fits of the spin−echo modulation for the summed intensity across each of the REINE 2D peaks. In this section, it is shown that a pixel-by-pixel fitting of the spin−echo modulation for the REINE 2D peaks reveals variations in the fitted *J* coupling constants that are correlated with changes in the ^{31}P chemical shifts of the coupled nuclei. The existence of such variations is evident from Figure 5, which presents REINE peaks obtained for the cadmium phosphate glass at τ_j values corresponding to the zero crossings observed in the spin−echo modulations for the summed intensities of the four REINE peaks (see Figure 4). While the summed intensities across the peaks are close to zero (less than 6.5% of the summed intensity for the REINE peak for $\tau_j = 0$), areas of significant positive and negative intensity are clearly identifiable. The interpretation in terms of the magnitude of the *J* coupling is straightforward: areas of negative and positive intensity correspond to an enhanced and reduced spin−echo modulation associated with areas of stronger and weaker *J* couplings, respectively. The intensity changes across the peaks indicate significant and systematic variations of the *J* couplings. For example, the intensity—normalized with respect to the $\tau_j = 0$ spectra—varies from approximately -6 to $+1$% and -4 to $+9$% over the P_1-P_1 and P_1-P_2 peaks, respectively.

A similar trend in the intensity profile is observed for each of the 2D REINE peaks shown in Figures 5a−5d; namely, areas of positive intensity are at the bottom, while areas of negative intensity are at the top of each peak. This suggests correlations between the *J* couplings and the chemical shifts of the bonded units. In this respect, it is to be noted that chemical-shift dependent variations in the $^2J_{P,P}$ couplings have been observed previously in a 2D ^{31}P MAS *z*-filtered spin−echo spectrum of a phosphate glass. In ref 34, Fayon et al. presented a 2D ^{31}P spin−echo spectrum of a lead phosphate glass, $0.66PbO-0.34P_2O_5$, where the splitting due to a $^2J_{P,P}$ coupling for the broad P_1 resonance is observed to increase from 17 to 20.5 Hz with decreasing ^{31}P chemical shift (increasing negative value).

However, it is to be emphasized that a pixel-by-pixel fitting of the *J* modulation for the 2D REINE peaks provides much greater insight: in the simple spin−echo experiment, the modulation of the signal intensity is only resolved on the basis of the ^{31}P SQ chemical shift; e.g., for a P_1 resonance, the observed time-domain curve is a superposition of contributions from P_1-P_1 and P_1-P_2 moieties. This is to be compared to the REINE experiment where the resolution of the 2D refocused INADEQUATE experiment enables the separate spin−echo modulation of, e.g., P_1-P_1 and P_1-P_2 moieties to be observed in a 2D fashion. For the cadmium phosphate glass studied here, we specifically note that there is no clearly evident chemical-shift variation in the *J* multiplet pattern (in particular for the P_1 resonance) in a 2D ^{31}P MAS *z*-filtered spin−echo spectrum (shown in Figure 1d).

As discussed above (see Figure 4 and Table 4 in section 4), the summed intensity for each of the four 2D REINE peaks is well fit to either eq 1 (P_1-P_1 and P_1-P_2) or eq 2 (P_2-P_1 and P_2-P_2), where eq 1 depends on one *J* coupling ($^2J_{P_1,P_1}$ for the P_1-P_1 2D REINE peak and $^2J_{P_1,P_2}$ for the P_1-P_2 2D REINE peak), while eq 2 depends on two *J* couplings ($^2J_{P_1,P_2}$ and $^2J_{P_2,P_2}$ for both the P_2-P_1 and P_2-P_2 2D REINE peaks). Figure 6, Figure 7, and Figure 8 show the six separate 2D variations in the respective *J* couplings obtained from a pixel-by-pixel fitting of the 2D REINE peaks to either eq 1 (P_1-P_1 and P_1-P_2) or eq 2 (P_2-P_1 and P_2-P_2). Specifically, 2D variations in the *J* couplings are shown for: $^2J_{P_1,P_1}$ in Figure 6 as determined for the fit of the P_1-P_1 2D REINE peak; $^2J_{P_1,P_2}$ in Figure 7 as determined for fits of the P_1-P_2 (7a, top row), P_2-P_1 (7e, middle

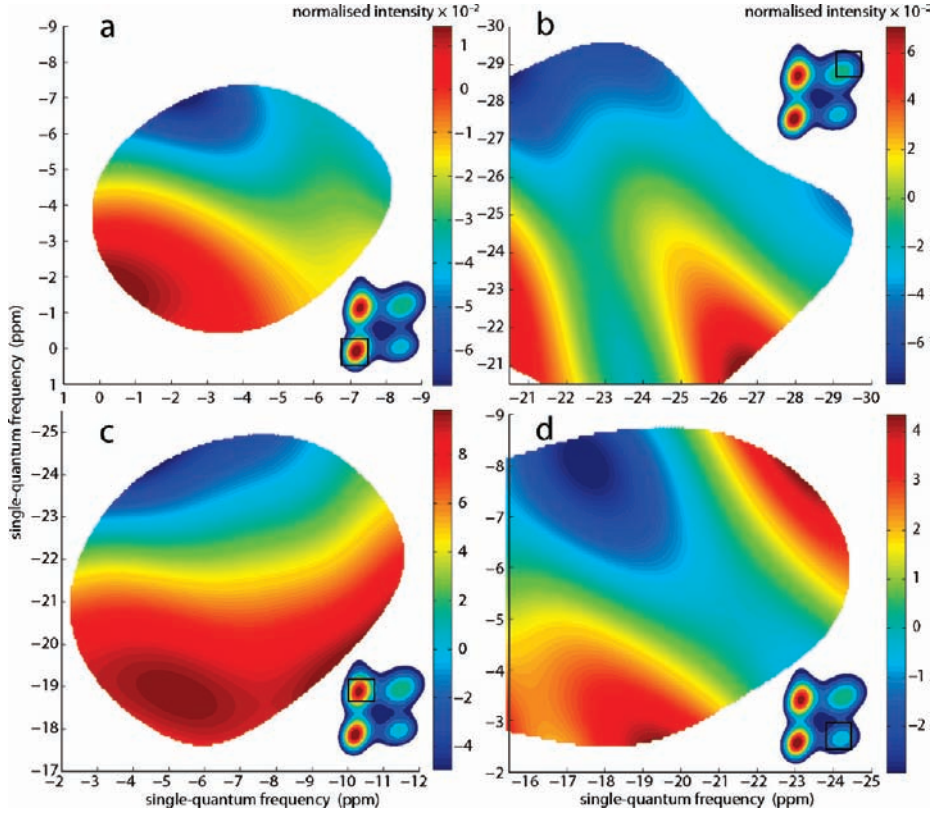

Figure 5. (a)−(d) ^{31}P (121.5 MHz) MAS NMR REINE spectra (in pseudo-COSY representation) of the cadmium phosphate glass for echo durations, τ_j, close to the respective (average) *J*-modulation zero-crossings: (a) P_1-P_1, $\tau_j = 18.0$ ms; (b) P_2-P_2, $\tau_j = 18.0$ ms; (c) P_1-P_2, $\tau_j = 14.4$ ms; (d) P_2-P_1, $\tau_j = 18.0$ ms. The areas shown correspond to those pixels for which the intensity at $\tau_j = 0$ exceeded 66%—for (a) and (c)—and 75%—for (b) and (d)—of the maximum intensity. Intensities are normalized, for each pixel, with respect to the corresponding intensity at $\tau_j = 0$.

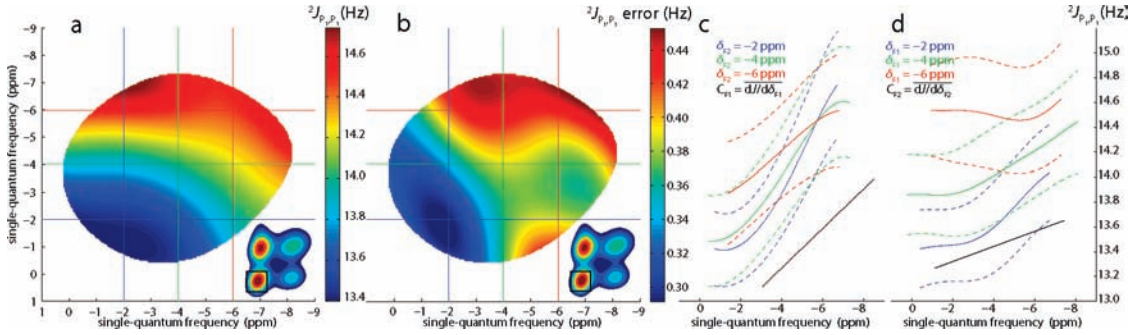

Figure 6. 2D variation of (a) the $^2J_{P_1,P_1}$ coupling and (b) associated fitting errors obtained for the cadmium phosphate glass by a pixel-by-pixel (10 pixels per ppm in both dimensions) fitting to eq 1 of the spin−echo modulation for the P_1-P_1 ^{31}P (121.5 MHz) MAS NMR REINE peak in pseudo-COSY representation. The area shown corresponds to those pixels for which the intensity at $\tau_j = 0$ exceeded 66% of the maximum intensity. Three selected (c) columns and (d) rows from the 2D $^2J_{P1,P1}$-coupling variation map in (a)—the dashed lines correspond to the error in the fitted $^2J_{P_1,P_1}$ coupling. The black lines indicate the gradients (c) $C_{F1} = dJ/d\delta_{F1}$ and (d) $C_{F2} = dJ/d\delta_{F2}$; as described in the text and tabulated in Table 5, these gradients correspond to the average pixel-by-pixel change in the *J* coupling with respect to the F_1 and F_2 chemical shift.

row), and P_2-P_2 (7i, bottom row) 2D REINE peaks; and $^2J_{P_2,P_2}$ in Figure 8 as determined for fits of the P_2-P_1 (8a, top row) and P_2-P_2 (8e, bottom row) 2D REINE peaks.

The first and second columns in Figure 6, Figure 7, and Figure 8 show color-coded 2D contour maps of the fitted *J* coupling (first column) and the associated fitting error (second column) for the specified region of the REINE spectrum (in pseudo-COSY SQ−SQ representation)—see the box in the insets showing the refocused INADEQUATE spectrum. To highlight the observed correlations between the fitted *J* couplings and the F_1 and F_2 ^{31}P chemical shifts, the two furthest right-hand columns in Figure 6, Figure 7, and Figure 8 show the variation of the fitted *J* couplings (together with the associated error bars as dashed lines) for three specific columns and rows, as extracted from the 2D distributions. The ^{31}P chemical shifts for the extracted columns and rows are indicated by vertical and horizontal lines in the contour maps in the two furthest left-hand columns.

For each 2D variation in the *J* couplings, the correlation with the F_1 (vertical) and F_2 (horizontal) ^{31}P chemical shifts was quantified using the following procedure. First, the pixel-by-pixel variation of the fitted *J* coupling was obtained by subtracting the fitted value for each pixel from that for the immediately adjacent pixel, separately for the F_1 and F_2 dimensions, to generate two arrays. The median (C_{F1} or C_{F2}) values along with their standard deviations ($\sigma(C_{F1})$ or $\sigma(C_{F2})$) are listed, together with the minimum, maximum, and average fitted *J* couplings, in Table 5 for each of the six 2D variations

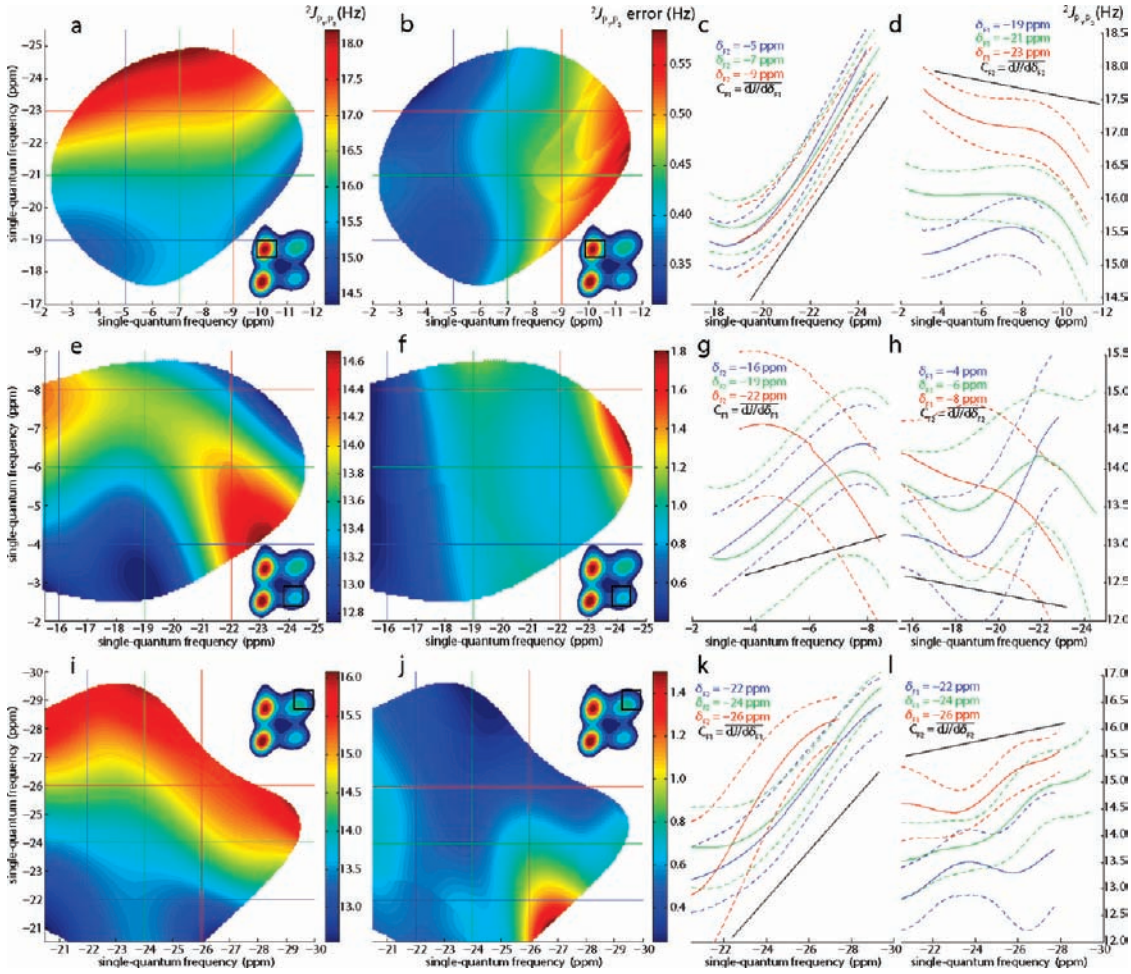

Figure 7. 2D variations of (a), (e), (i) the $^2J_{P_1,P_2}$ coupling and (b), (f), (j) associated fitting errors obtained for the cadmium phosphate glass by a pixel-by-pixel (10 pixels per ppm in both dimensions) fitting of the spin−echo modulation for the (a), (b) P_1-P_2 (fit to eq 1), (e), (f) P_2-P_1 (fit to eq 2), and (i), (j) P_2-P_2 (fit to eq 2) ^{31}P (121.5 MHz) MAS NMR REINE peaks in pseudo-COSY representation. The areas shown correspond to those pixels for which the intensity at $\tau_j = 0$ exceeded 66%—for (a)—or 75%—for (e) and (i)—of the maximum intensity. Three selected (c), (g), (k) columns and (d), (h), (l) rows from the corresponding 2D variation maps—the dashed lines correspond to the error in the fitted $^2J_{P_1,P_2}$ coupling. The black lines indicate the gradients (c), (g), (k) $C_{F1} = dJ/d\delta_{F1}$ and (d), (h), (l) $C_{F2} = dJ/d\delta_{F2}$; as described in the text and tabulated in Table 5, these gradients correspond to the average pixel-by-pixel change in the J coupling with respect to the F_1 and F_2 chemical shift.

in the J couplings. The standard deviations ($\sigma(C_{F1})$ or $\sigma(C_{F2})$) are found to correspond to the average error in the fitted $^2J_{P,P}$ coupling. (Histogram plots for each array are shown in the Supporting Information.) Quantitatively, for a change of +1 ppm in the direct and indirect dimensions, the J coupling changes—on average—by C_{F2} and C_{F1} Hz, respectively.

As stated in Table 5, the fitted $^2J_{P_1,P_1}$ coupling varies from 13.4 to 14.8 Hz across the P_1-P_1 2D REINE peak—note that this change is significant compared to the fitting errors (≤0.5 Hz). This can be compared to the $^2J_{P_1,P_1}$ couplings determined for P_2O_7 groups in crystalline compounds: SnP_2O_7 16−19.5 Hz (2D z-filtered spin echo);[45] $Zn_2P_2O_7$ 21 Hz (observed zero crossing in build-up of refocused INADEQUATE signal);[33] $Cd_2P_2O_7$ 23 ± 4 Hz,[79] SiP_2O_7 17 ± 1 and 23 ± 1 Hz,[80] $Na_4P_2O_7 \cdot 10H_2O$ 19.5 ± 2.5 Hz,[81] and TiP_2O_7 18 ± 2, 21 ± 2, and 31 ± 2 Hz[82] (TOBSY[83] build-up curves).

Considering the variation in the $^2J_{P_1,P_1}$ coupling (see Figure 6a), the most evident trend is the increase in $^2J_{P_1,P_1}$ for increasingly negative ^{31}P chemical shifts in the F_1 (vertical) dimension. By comparison, the trend in the F_2 (horizontal) dimension is less marked. This is reflected in a larger correlation with the F_1 chemical shift ($C_{F1} = -0.16$ Hz/ppm) as compared to the F_2 correlation ($C_{SQ} = -0.06$ Hz/ppm). This shows, for the cadmium phosphate glass studied here, that the magnitude of the J coupling in a P_1-P_1 dimer is more sensitive to the chemical shift of the neighboring ^{31}P nucleus as compared to the ^{31}P chemical shift of the nucleus directly observed in the F_2 dimension.

For the $^2J_{P_1,P_2}$ coupling (see Figure 7), the fitted J couplings are in the range 15.0 ± 0.3 to 18.2 ± 0.3 Hz for the P_1-P_2 peak (Figure 7a), 12.7 ± 0.5 to 14.7 ± 0.5 Hz for the P_2-P_1 peak (Figure 7e), and 12.6 ± 0.9 to 16.1 ± 0.5 Hz for the P_2-P_2 peak (Figure 7i). Given these small discrepancies

(79) Dusold, S.; Kummerlen, J.; Sebald, A. *J. Phys. Chem. A* **1997**, *101*, 5895–5900.
(80) Iuliucci, R. J.; Meier, B. H. *J. Am. Chem. Soc.* **1998**, *120*, 9059–9062.
(81) Dusold, S.; Milius, W.; Sebald, A. *J. Magn. Reson.* **1998**, *135*, 500–513.
(82) Helluy, X.; Marichal, C.; Sebald, A. *J. Phys. Chem. B* **1998**, *104*, 2836–2845.
(83) Baldus, M.; Meier, B. H. *J. Magn. Reson. A* **1996**, *121*, 65–69.

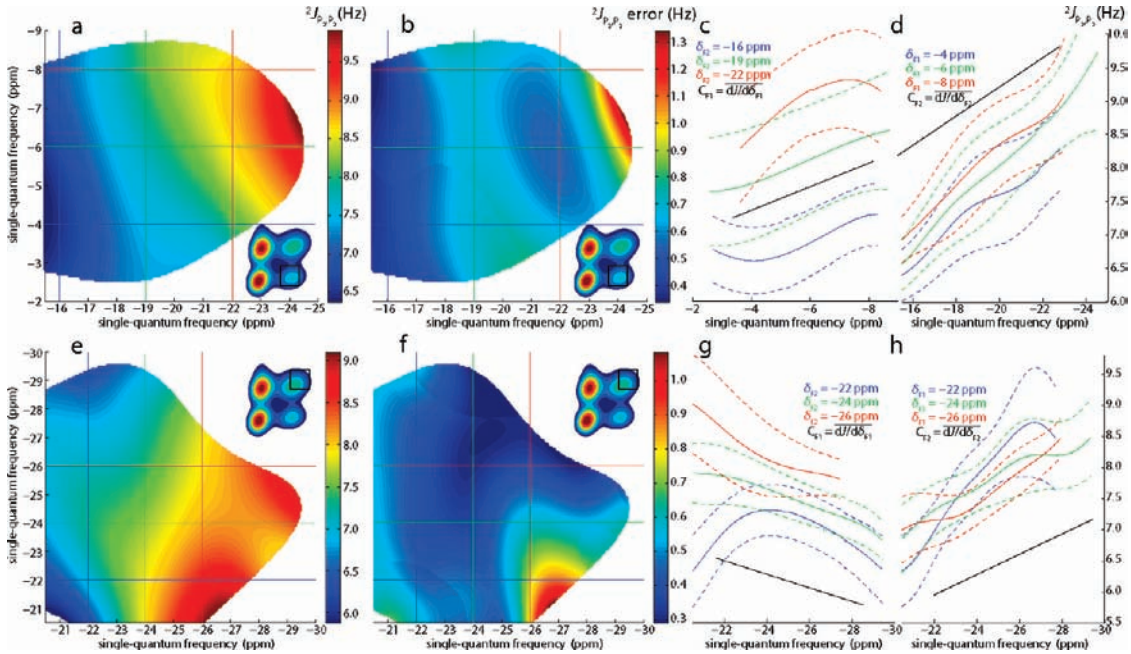

Figure 8. 2D variations of (a), (e) the $^2J_{P_2,P_2}$ coupling and (b), (f) associated fitting errors obtained for the cadmium phosphate glass by a pixel-by-pixel (10 pixels per ppm in both dimensions) fitting to eq 2 of the spin−echo modulation for the (a), (b) P_2-P_1 and (e), (f) P_2-P_2 ^{31}P (121.5 MHz) MAS NMR REINE peaks. The areas shown correspond to those pixels for which the intensity at $\tau_j = 0$ exceeded 75% of the maximum intensity. Three selected (c), (g) columns and (d), (h) rows from the corresponding 2D variation maps—the dashed lines correspond to the error in the fitted $^2J_{P_2,P_2}$ coupling. The black lines indicate the gradients (c), (g) $C_{F1} = dJ/d\delta_{F1}$ and (d), (h) $C_{F2} = dJ/d\delta_{F2}$; as described in the text and tabulated in Table 5, these gradients correspond to the average pixel-by-pixel change in the J coupling with respect to the F_1 and F_2 chemical shift.

Table 5. Minimum, Maximum, and Average $^2J_{P,P}$ Couplings, together with Measures of Their Variation with Respect to the F_1 and F_2 Frequencies, as Extracted from Fits of the Spin−Echo Modulation for the 2D REINE Peaks

	Hz			× 10^{-2} Hz/ppm			
J coupling and REINE peak	avg. J^a	min. J^b	max. J^b	$C_{F1}{}^c$	$\sigma(C_{F1})^c$	$C_{F2}{}^c$	$\sigma(C_{F2})^c$
$^2J_{P_1,P_1}$ (P_1-P_1, Figure 6)	14.0 ± 0.4	13.4 ± 0.3	14.8 ± 0.5	−15.9 ± 0.3	41.3	−6.1 ± 0.3	39.5
$^2J_{P_1,P_2}$ (P_1-P_2, Figure 7)	16.3 ± 0.4	15.0 ± 0.3	18.2 ± 0.3	−52.7 ± 0.3	46.8	6.1 ± 0.3	44.0
$^2J_{P_1,P_2}$ (P_2-P_1, Figure 7)	13.5 ± 0.8	12.7 ± 0.5	14.7 ± 0.5	−12.3 ± 0.8	99.1	7.4 ± 0.8	94.8
$^2J_{P_1,P_2}$ (P_2-P_2, Figure 7)	14.3 ± 0.4	12.6 ± 0.9	16.1 ± 0.5	−46.3 ± 0.4	59.7	−12.1 ± 0.4	59.1
$^2J_{P_2,P_2}$ (P_2-P_1, Figure 8)	7.7 ± 0.6	6.4 ± 0.4	9.9 ± 1.3	−17.8 ± 0.8	92.2	−29.8 ± 0.7	91.7
$^2J_{P_2,P_2}$ (P_2-P_2, Figure 8)	7.4 ± 0.3	5.9 ± 0.6	9.1 ± 0.9	13.5 ± 0.4	52.8	−24.0 ± 0.4	50.5

[a] The average J couplings as determined in section 4 for fits of the spin−echo modulation of the summed intensity for each REINE peak. [b] The minimum and maximum J couplings extracted from a pixel-by-pixel fitting for the peak areas shown in Figure 6, Figure 7, and Figure 8. [c] The median values and standard deviations of arrays (see Supporting Information for histogram plots) produced by subtracting the fitted J coupling for each pixel from that for the immediately adjacent pixel, along F_1 and F_2, i.e., C_{F1} and C_{F2} correspond to the average pixel-by-pixel change in the J coupling with respect to the F_1 (vertical) and F_2 (horizontal) chemical shifts, respectively.

between the distributions for the three 2D REINE peaks, it is instructive to compare the average uncertainties associated with each 2D distribution in Figure 7: ∼0.4, 0.7, and 0.9 Hz for the P_1-P_2, P_2-P_2, and P_2-P_1 2D REINE peaks, respectively. The smaller average error for the P_1-P_2 REINE peak is a consequence of the simpler fitting function; indeed, eq 1 depends on only one J coupling, whereas eq 2 depends on two J couplings. Compare also the magnitude of the correlation coefficients—listed in Table 4—for the fits in section 4 to the spin−echo modulations for summed intensities across the corresponding 2D REINE peaks. In conclusion, by virtue of smaller associated errors and correlation coefficients, Figure 7a provides the most accurate measure of the variation of the J coupling between P_1 and P_2 units in the glass.

Upon inspection of the fitted $^2J_{P_1,P_2}$ couplings for the P_1-P_2 2D REINE peak, the most evident trend is the marked increase in $^2J_{P_1,P_2}$ for increasingly negative ^{31}P chemical shifts in the F_1 (vertical) dimension, i.e., corresponding to the chemical shift of the P_2 nucleus that is bonded (via a P−O−P linkage) to a P_1 nucleus. This is reflected in the large correlation with the F_1 chemical shift ($C_{F1} = -0.53$ Hz/ppm), with this being over three times as large as that for the P_1-P_1 2D REINE peak ($C_{F1} = -0.16$ Hz/ppm). By contrast, there is no clear trend in the F_2 (horizontal) dimension ($C_{F2} = +0.06$ Hz/ppm); i.e., the $^2J_{P_1,P_2}$ coupling only has a weak dependence on the ^{31}P chemical shift of the observe P_1 nucleus.

With respect to the J coupling ($^2J_{P_1,P_1}$ or $^2J_{P_1,P_2}$) of a P_1 unit, the REINE experiment has revealed a marked dependence with respect to the ^{31}P chemical shift of the neighboring ^{31}P nucleus, i.e., as observed in a change in the fitted J coupling in the F_1 (vertical) dimension. It is to be emphasized that such a change cannot be observed in a 2D z-filtered spin−echo spectrum. Indeed, the absence of any evident change in the doublet pattern observed for the P_1 resonance in the 2D z-filtered spin−echo spectrum of the cadmium phosphate glass presented in Figure 1d is consistent with the absence of a marked correlation in the F_2 (horizontal) dimension for either the P_1-P_1 or P_1-P_2 2D REINE peaks: the C_{F2} coefficients for the two 2D peaks have the same small magnitude (0.06 Hz/ppm). Indeed, their opposite

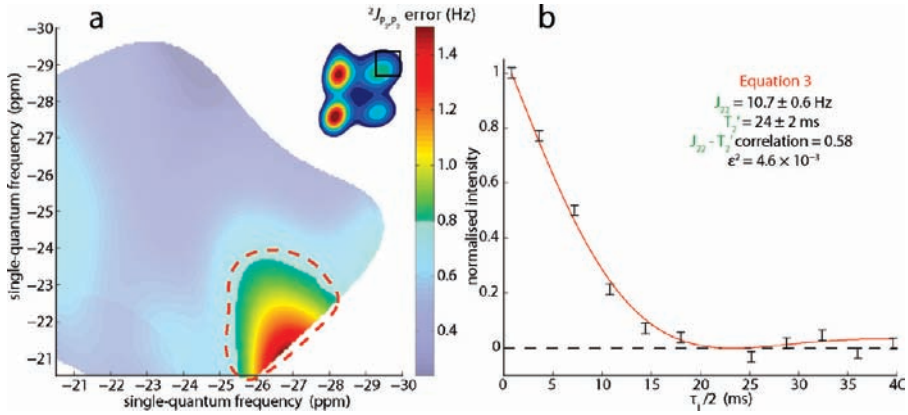

Figure 9. (a) 2D variations of the errors on the $^2J_{P_1,P_2}$ coupling, as determined from the fitting to eq 2 of the P_2-P_2 peak for the 2D ^{31}P (121.5 MHz) MAS NMR REINE spectra of the cadmium phosphate glass in pseudo-COSY representation. The area shown corresponds to those pixels for which the intensity at $\tau_j = 0$ exceeded 75% of the maximum intensity. The fitting errors increase dramatically in the bottom right-hand corner. (b) Fits using eq 3 of the spin−echo modulation of the summed signal intensity, for the area—highlighted in (a) within the dashed red line—for which the uncertainties exceeded 0.8 Hz.

signs would lead to a canceling out of any trend for the individual $^2J_{P_1,P_1}$ or $^2J_{P_1,P_2}$ coupling since the simple spin−echo experiment does not distinguish between the modulation due to the separate J couplings.

Finally, the fitted J couplings for the 2D REINE peaks at the P_2 chemical shift are considered. The same trend as discussed above for the P_1-P_2 2D REINE peak is evident for the fitted $^2J_{P_1,P_2}$ couplings for the P_2-P_2 2D REINE peak: a marked increase in $^2J_{P_1,P_2}$ for increasingly negative ^{31}P chemical shifts in the F_1 (vertical) dimension, i.e., corresponding to the chemical shift of the P_1 nucleus that is bonded to a P_2 nucleus, while there is no evident trend in the F_2 (horizontal) dimension, i.e., no clear dependence on the ^{31}P chemical shift of the observed P_2 nucleus. (For the $^2J_{P_1,P_2}$ couplings at the P_2-P_1 2D REINE peak, the fitting errors are larger, and there are no clear trends in the changes with respect to either the F_1 or F_2 dimension.) Considering the $^2J_{P_2,P_2}$ coupling variations, for both the P_2-P_1 and P_2-P_2 2D REINE peaks, there is a moderate increase with respect to the F_2 (horizontal) dimension: $C_{F2} = -0.30$ and -0.24 Hz/ppm.

In summary, it is to be noted that the ranges of the J-coupling distributions are approximately 10, 20, and 40% of the median value for the $^2J_{P_1,P_1}$, $^2J_{P_1,P_2}$, and $^2J_{P_2,P_2}$ couplings, respectively. This highlights the importance of using the REINE approach, which is sensitive both to the variance and the mean of each J-coupling constant, to identify these experimental trends.

6. Two-Dimensional ^{31}P NMR REINE Experiments: Evidence for Longer Chain Lengths

For the P_2-P_2 2D REINE peak, it was shown in section 4 that the spin−echo modulation for the summed intensity is well fit to eq 2, i.e., corresponding to the presence of tetraphosphate chains. Moreover, the J-coupling variations determined for the P_2-P_2 2D REINE peak, as presented in the above section, result from fits of the pixel-by-pixel spin−echo modulation to eq 2.

Complications—which would lead to an increase in fitting errors—may arise from the presence of longer chains (five or more tetrahedra) or ring structures. As described above, the analysis of the summed modulations for each peak gave no indication for their presence. However, it is feasible that a small proportion of chains with these different make-ups could exist but may not be detected due to the predominance of signal from tetraphosphate chains. Table 2 and Table 3 show that these would lead to a $\cos^2$ modulation of the P_2-P_2 peak. For the bottom right-hand corner of the P_2-P_2 2D REINE peak (see the area highlighted in Figure 9a), the fitted $^2J_{P_2,P_2}$ coupling shown in Figure 8e is of similar strength to the fitted $^2J_{P_1,P_2}$ coupling (Figure 7i). Moreover, the fitting errors become large, with this being a consequence of the two J-coupling parameters being similar and hence interchangeable for this region. Indeed, Figure 9 shows that fitting the summed intensity for the area where the fitting error for the $^2J_{P_1,P_2}$ coupling is greater than 0.8 Hz to the $\cos^2$ function of eq 3 gives good fits with an average J coupling of 10.0 ± 0.6 Hz, respectively. This is consistent with the presence of longer chains (5+) and/or phosphate rings in the cadmium phosphate glass. For the P_2-P_2 2D REINE peak, the identification of longer chains or rings for the bottom right-hand corner, i.e., for the most negative ^{31}P chemical shifts, is consistent with the interpretation of 2D DQ−SQ correlation spectra by Witter et al.[28] and Fayon et al.,[34] where P_2 resonances with the most negative chemical shifts are assigned to P_2 phosphate units with two P_2 neighbors. Furthermore, in Figure 7 of ref 35, the TQ coherence due to a $P_2-P_2-P_2$ linkage is clearly shown to correspond to a more negative ^{31}P chemical shift than that for a $P_1-P_2-P_2$ or a $P_1-P_2-P_1$ linkage. It is also to be noted that Alam has shown that ring formation can also lead to a change to a more negative ^{31}P chemical shift.[84]

7. Summary and Outlook

While solid-state NMR is inherently suited to the structural characterization of disordered solids, the observation of broad Gaussian-like lineshapes seemingly indicates a restricted extractable information content. However, the observation of correlations in chemical shifts between neighboring spins in two-dimensional refocused INADEQUATE MAS NMR spectra has previously been shown to provide high resolution for a diphenylphosphino-amine and a cellulose sample.[85] Moreover, Cadars et al. have shown how two-dimensional conditional probability distributions can be extracted from such 2D refocused INADEQUATE MAS NMR spectra of disordered solids.[73,75,76]

(84) Alam, T. M. *Int. J. Mol. Sci.* **2002**, *3*, 888–906.
(85) Sakellariou, D.; Brown, S. P.; Lesage, A.; Hediger, S.; Bardet, M.; Meriles, C. A.; Pines, A.; Emsley, L. *J. Am. Chem. Soc.* **2003**, *125*, 4376–4380.

This paper has considered a representative phosphate glass, where broad featureless 2D peaks are observed in a ^{31}P refocused INADEQUATE spectrum; indeed, a conditional probability analysis using the protocol of Cadars et al.[73] indicates that that there is no evident correlation between the ^{31}P chemical shifts of bonded phosphate units; e.g., a P_1 unit resonating at a particular chemical shift has an approximately equal probability of being linked to any of the P_2 tetrahedra and vice versa. In spite of this absence of any correlation between the chemical shifts of ^{31}P nuclei in bonded phosphate groups, it has been shown here that the appending of a spin−echo to the refocused INADEQUATE experiment[38]—we refer to this as the REINE (Refocused INADEQUATE spin−Echo) experiment—yields variations of the $^2J_{P,P}$ couplings that exhibit clear correlations with the ^{31}P chemical shifts of the coupled nuclei. The observation of separate variations for each ^{31}P REINE peak and the 2D nature of the REINE experiment yield new information that is not observable in previously presented 2D z-filtered ^{31}P spin−echo spectra.[34,52]

How can the observations for the phosphate glass considered here be explained, namely, that, on the one hand, there is no evident correlation between the chemical shifts of ^{31}P nuclei in bonded phosphate groups but, on the other hand, there are clear 2D correlations between the $^2J_{P,P}$ couplings and the ^{31}P chemical shifts of the coupled nuclei? Consider the case of the bonded P_1 and P_2 units, each with a distribution of ^{31}P chemical shifts. The first observation implies that there is no propensity for a particular P_1 unit to be bonded to a specific P_2 unit, such that all P_1 nuclei are bonded to all P_2 nuclei and vice versa; i.e., there is no evident next-nearest-neighbor ordering in the studied glass. (This is consistent with Monte Carlo simulations of phosphate glasses that show that phosphate polyhedron connectivity is best described by a random distribution of next-nearest-neighbor connectivities.[86]) However, the second observation is revealing that there *is* a variation in the $^2J_{P1,P2}$ coupling with respect to the 2D distribution of ^{31}P chemical shifts of the P_1 and P_2 units. Specifically, Figure 7 reveals, for the glass studied here, that the $^2J_{P_1,P_2}$ coupling exhibits a marked dependence on the chemical shift of the ^{31}P nucleus to which a specific nucleus is coupled.

The interpretation of such changes in measured J couplings in terms of structural changes (e.g., bond angle variations) is complicated by there being four distinct contributions to a J coupling, namely, Fermi-contact, spin-dipole, paramagnetic, and diamagnetic terms.[87,88] As a consequence, first-principles calculations of J couplings are very helpful in aiding structural interpretation.[89] Recently, a first-principles theory for calculating J couplings in extended systems based on density-functional theory and formulated within a planewave−pseudopotential framework[87] has been shown to be applicable for the calculation of J couplings in inorganic[87] and organic solids.[63,90] (This computational approach is currently being applied by our collaborators to the calculation of $^2J_{P,P}$ couplings in crystalline phosphates, and results will be presented in due course.) In the context of disordered solids, the combination of experimental NMR and calculation is already proving very useful: NMR chemical shifts and quadrupolar parameters have been calculated, e.g., for sodium silicate[91] and calcium aluminosilicate glasses,[92] while new insight into the still controversial structure of the prototypical glass former B_2O_3 has been provided by the comparison with experiment of ^{11}B chemical shifts as calculated for structures obtained by molecular dynamics simulation.[15,17]

The approach presented here has applicability beyond ^{31}P NMR of phosphate glasses. As well as ^{13}C NMR of natural and synthetic polymers, e.g., cellulose,[38] ^{29}Si two-dimensional DQ NMR spectra have been presented for zeolites, silicate glasses, surfactant-templated silicate layers, and Bioceramics.[75,93−101] Moreover, Lo and Edén have recently presented a ^{27}Al (spin $I = (5/2)$) DQ MAS spectrum of a lanthanum aluminate glass using a symmetry-based homonuclear dipolar recoupling technique to create DQ coherence between two half-integer quadrupolar nuclei.[102] In this context, it is to be noted that a $^2J_{O,O}$ coupling of 7.9 Hz has recently been measured in a ^{17}O (spin $I = 5/2$) MAS NMR spin−echo experiment for ^{17}O-labeled glycine·^{2}HCl.[63] Concerning further ^{31}P experiments, better separation of the J modulation for different connectivities of phosphate tetrahedra (e.g., $P_1-P_2-P_1$, $P_1-P_2-P_2$, and $P_2-P_2-P_2$) could be achieved by appending a spin−echo onto ^{31}P TQ experiments.[35]

The observation of experimental J coupling and chemical-shift correlations for the apparently featureless peaks in 2D solid-state NMR spectra of disordered glasses establishes a potentially rich source of structural information. Specifically, there is much scope for using first-principles calculations to compare experimental J-coupling and chemical-shift correlations—as revealed by REINE MAS NMR spectra as well as those provided by, e.g., ^{17}O NMR[103]—with those derived from glass structures calculated using molecular dynamics simulations. Such a combined experimental and calculation approach is essential if characteristic structure−function relationships of advanced multicomponent glasses are to be identified.

Acknowledgment. Support from the EPSRC is acknowledged. We thank Sylvian Cadars and Paul Hodgkinson for making available their fitting routines. Helpful discussions with Sylvian Cadars,

(86) Brow, R. K.; Click, C. A.; Alam, T. M. *J. Non-Cryst. Solids* **2000**, *274*, 9–16.
(87) Joyce, S. A.; Yates, J.; Pickard, C. J.; Mauri, F. *J. Chem. Phys.* **2007**, *127*, 204107.
(88) Cremer, D.; Grafenstein, J. *Phys. Chem. Chem. Phys.* **2007**, *9*, 2791–2816.
(89) Krivdin, L. B.; Contreras, R. H. *Annu. Rep. Nucl. Magn. Reson. Spectrosc.* **2007**, *61*, 133–245.
(90) Joyce, S. A.; Yates, J. R.; Pickard, C. J.; Brown, S. P. *J. Am. Chem. Soc.* **2008**, *130*, 12663–12670.
(91) Charpentier, T.; Ipsas, S.; Profeta, M.; Mauri, F.; Pickard, C. J. *J. Phys. Chem. B* **2004**, *108*, 4147–4161.
(92) Benoit, M.; Profeta, M.; Mauri, F.; Pickard, C. J.; Tuckerman, M. E. *J. Phys. Chem. B* **2005**, *109*, 6052–6060.
(93) Fyfe, C. A.; Grondey, H.; Feng, Y.; Kokotailo, G. T. *Chem. Phys. Lett.* **1990**, *173*, 211–215.
(94) Glock, K.; Hirsch, O.; Rehak, P.; Thomas, B.; Jäger, C. *J. Non-Cryst. Solids* **1998**, *232*, 113–118.
(95) Olivier, L.; Yuan, X.; Cormack, A. N.; Jäger, C. *J. Non-Cryst. Solids* **2001**, *293*, 53–66.
(96) Hedin, N.; Graf, R.; Christiansen, S. C.; Gervais, C.; Hayward, R. C.; Eckert, J.; Chmelka, B. F. *J. Am. Chem. Soc.* **2004**, *126*, 9425–9432.
(97) Brouwer, D. H.; Kristiansen, P. E.; Fyfe, C. A.; Levitt, M. H. *J. Am. Chem. Soc.* **2005**, *127*, 542–543.
(98) Brouwer, D. H.; Darton, R. J.; Morris, R. E.; Levitt, M. H. *J. Am. Chem. Soc.* **2005**, *127*, 10365–10370.
(99) Wiench, J. W.; Lin, V. S.-Y.; Pruski, M. *J. Magn. Reson.* **2008**, *193*, 233–242.
(100) Rawal, A.; Wei, X.; Akinc, A.; Schmidt-Rohr, K. *Chem. Mater.* **2008**, *20*, 2583–2591.
(101) Cadars, S.; Brouwer, D. H.; Chmelka, B. F. *Phys. Chem. Chem. Phys.* **2009**, *11*, 1825–1837.
(102) Lo, A. Y. H.; Edén, M. *Phys. Chem. Chem. Phys.* **2008**, *44*, 6635–6644.
(103) Clark, T. M.; Grandinetti, P. J.; Florian, P.; Stebbins, J. F. *Phys. Rev. B* **2004**, *70*, 064202.

Lyndon Emsley, Ray Dupree, Diane Holland, Nathan Barrow, Johanna Becker-Baldus, and Amy Webber are acknowledged. The authors are grateful to the anonymous reviewers for their constructive suggestions.

Supporting Information Available: ^{31}P refocused INADEQUATE spectrum (in DQ−SQ representation) of the cadmium phosphate glass; a full phase cycle for the REINE experiment; conditional probability maps for the P_1-P_1, P_2-P_1, and P_2-P_2 pseudo-COSY peaks; parameters obtained from additional fits of the REINE data; analytical simulations of spin−echo modulations for a distribution of J couplings; numerical density-matrix simulations of REINE modulation for $n = 0$ rotational resonance; an analysis of the T_2'−chemical-shift correlations for the 2D REINE peaks; histogram plots of the distributions of the J-coupling−chemical-shift and T_2'−chemical-shift correlation coefficients; complete ref 55. This material is available free of charge via the Internet at http://pubs.acs.org.

JA902238S